Environ. Eng. Res. 2018; 23(1): 1-9
https://doi.org/10.4491/eer.2016.158

pISSN 1226-1025
eISSN 2005-968X

Potential degradation of methylene blue (MB) by nano-metallic particles: A kinetic study and possible mechanism of MB degradation

Jiwan Singh[1†], Yoon-Young Chang[2], Janardhan Reddy Koduru[2†], Jae-Kyu Yang[3]

[1]*Department of Environmental Science, Babasaheb Bhimrao Ambedkar University, Lucknow-226025, India*
[2]*Department of Environmental Engineering, Kwangwoon University, Seoul 01897, Republic of Korea*
[3]*Ingenium College of Liberal Arts, Kwangwoon University, Seoul 01897, Republic of Korea*

ABSTRACT

The degradation of methylene blue (MB) in an aqueous solution by nano-metallic particles (NMPs) was studied to evaluate the possibility of applying NMPs to remove MB from the wastewater. Scanning electron microscopy (SEM), Fourier-transform infrared (FTIR) spectroscopy and X-ray photoelectron spectroscopy (XPS) were used to characterize the synthesized NMPs before and after the reaction. The effects of the NMP dosage, the initial pH, the initial concentration of MB and the amount of H_2O_2 on the MB degradation outcomes were studied. The highest removal rate of MB was achieved to be 100% with an initial MB concentration of 5 mg/L, followed by 99.6% with an initial concentration of 10 mg/L under the following treatment conditions: dose of NMP of 0.15 g/L, concentration of H_2O_2-100 mM and a temperature of 25°C. The SEM analysis revealed that the nano particles were not spherical in shape. FTIR spectra shows occurrence of metal oxides on the surfaces of the NMPs. The XPS analyses results represent that Fe, Zn, N, Ca, C and O were occurred on the surfaces of the NMPs. The degradation of MB was suitable for the pseudo-first-order kinetics.

Keywords: Degradation, Kinetics, MB, Mechanism, NMPs, SEM

1. Introduction

Colors are extensively used in the chemical industry. However, industrial applications of colors are also increasing steadily, which leading to increase water pollution [1]. In fact, the presence of a very small amount of dye in water (< 1 mg/L for some dyes) is highly visible and enough to present an aesthetic problem [2]. Organic compounds such as dyes are harmful to humans who are in continued contact with them. It has been estimated that approximately 15% of the dyes of the total world manufacture are lost during the printing and dyeing processes which is discharged into water [3]. Methylene blue (MB), the most common dye in effluents from the textile, paper and printing industries, is often found in most industrial wastewater. The complete removal of MB is difficult due to the presence of aromatic rings in the structures which comprise the chromophore and polar groups in this wastewater [4, 5].

A removal efficiency of MB through adsorption by lotus leaf was 95.1% [6]; however, removal efficiency of MB by adsorption/photocatalytic degradation by nanocomposite pectin Zr(IV) selenotungstophosphate was reported to be 89.2% [7]. A degradation of efficiency of MB by nano zero valent iron (nZVI) assembled on magnetic Fe_3O_4/reduced graphene oxide was 98.0% [8]. The removal of MB through a chemical oxidation process which involves the application of nano-sized materials has proven to be particularly effective, mainly due to its simplicity and efficiency. Oxidation of organic pollutants by nano size ZVI found to be highly effective in wastewater treatment because of its better capability to decrease and stabilize various types of organic pollutants at small operating cost [9]. The zero-valent metals (ZVMs) having greater efficiency of producing reactive oxygen species, which mainly depends on the superficial transfer of electrons to dioxygen [10]. Therefore, the degradation of toxic dyes by nZVI has attracted much attention [11-12].

Received December 23, 2016 **Accepted** June 27, 2017

† Corresponding author
Email: jiwansingh95@gmail.com, reddyjchem@gmail.com
Tel: +91-522-2995606, +82-2-940-5496

Currently, oxidation processes have become promising techniques for the treatment of organic pollutants in wastewater [12]. Hydroxyl radicals are generated when the oxidation process uses prospective oxidants such as hydrogen peroxide and ozone. Presently, the preparation of nano zero valent metal (nZVMs) particles through liquid-phase reduction methods has been applied, during which sodium borohydride and metals salts are used. However, this method has a high preparation cost and can limit the application of nZVMs for the degradation of organic pollutants in water [13].

An advanced oxidation process (AOP) is one of the most promising technique for the degradation of organic pollutants through the production of reactive oxygen species (ROS) such as hydroxyl radical (•OH) [3]. This radical is as the key intermediate of Fenton process and high oxidative in nature. The •OH can oxidize attack almost all the organic compounds, and finally leading to the formation of mineral end-products [14]. Consequently, the activation of molecular oxygen occurs which to produce ROS for the oxidation of organic pollutants by nZVMs [15].

On the other hand, the metal-containing extracted solution of automobile shredder residue (ASR) is very useful for the synthesis of nano-metallic particles (NMPs). The concentrations of heavy metals in ASR are as follows: Zn-5,571.3 mg/kg, Cu-1,957.1 mg/g, Mn-1,068.8 mg/kg, Fe-151.8 g/kg, Ni-95.9 mg/kg, Pb-1,202.8 mg/kg and Cr-98.3 mg/kg [16].

At present, ASR waste contaminated with heavy metals is dumped into landfills in many countries, increasing the potential risk to humans through groundwater pollution [12-13]. The fine fraction of ASR is considered as a highly hazardous material due to presence of high concentrations of heavy metals [17]. It may be possible to prepare NMPs by utilizing a leachate of ASR waste to decrease the production cost and pollution load into groundwater. The degradation of MB by nZVI [18-20] has been reported. However, the degradation of MB using NMPs has yet to be reported.

Therefore, the present study is an attempt to degrade MB in the NMPs/H_2O_2 system by comparing the kinetics and/or the magnitude of MB discoloration. The effects of various factors (pH values, NMP dosages, initial concentrations of MB and the amounts of H_2O_2) on the rate of MB degradation are also discussed.

2. Materials and Methods

2.1. Leaching Experiment

The extraction of heavy metals from the fine fraction of ASR (< 0.25 mm) was carried out with 1.0 M of nitric acid at an L/S ratio (liquid/solid) of 10 mL/g and ultrasonic power of 500W. To increase the extraction of metals from the ASR, an ultrasonic generator (VCX-500, Sonics & Materials, Inc., USA) with a titanium probe was used. The ASR sample (50 grams) was mixed with 500 mL of the acid solution (1.0 M) in a 1,000 mL beaker and stirred with a thermostatic magnetic stirrer during 1 h ultrasonic treatment. The mixture was separated by using 0.45 μm filter paper.

2.2. Preparation of Nano-metallic Particles (NMPs)

The synthesis of NMPs from the extracted solution of ASR was carried out at a neutral pH. In this case, 100 mL of the extracted solution was placed into a 500-mL beaker and the pH of the solution was adjusted to 7 using 1.0 M of NaOH. The preparation of the NMPs was carried out through a reduction method [21]. A solution of 0.1 M $NaHB_4$ was added to the extracted solution of ASR at 40 drops/min while stirring using a temperature-controlled magnetic stirrer at 25 ± 0.5°C. The metal ions were rapidly converted into NMPs. The color of the mixture changed to black after the complete addition of the $NaHB_4$ solution. The prepared NMPs were separated by centrifugation at 3,667 × g for 30 min and were then washed several times with distilled water, followed by washing with ethyl alcohol to remove the extra $NaHB_4$ from the surfaces of the NMPs. After washing and separating the NMPs from the mixture, they were dried in a vacuum at 50°C. The metallic ions rapidly changed into NMPs with the addition of a $NaHB_4$ solution, as represented by Eq. (1) [13],

$$M^{+}/M^{2+}/M^{3+}{}_{(aq)} + BH_4^{-}{}_{(aq)} + H_2O \rightarrow NMPs_{(S)} + B(OH)_3(aq) + H_2\uparrow \quad (1)$$

where M represents the metal ions.

2.3. Experimental Design for MB Degradation

MB degradation by NMPs was conducted in 250 mL conical flasks at 25°C. This experiment was carried in a horizontal water bath shaker (SWB-35, Hanyang Scientific Equipment Co., Ltd., South Korea) at 50 rpm. Here, 100 mL of the MB solution was placed into a flask containing appropriate amounts of NMPs and H_2O_2. The pH of the MB solution was maintained with HCl (0.1 N) and NaOH (0.1 N) to check the effects of different pH levels on the MB degradation by NMPs. A pH meter (Orion 3 Star, Thermo Scientific) was used to measure the solution pH. To measure the residual MB concentration, samples were taken at various time intervals and were filtered through 0.25 μm filter paper. UV–visible spectrophotometer (UV 1601, Shimadzu) was used to determine the residual MB concentration in the solution at a maximum wavelength (λ_{max}) of 665 nm.

2.4. Instrumental Analysis of NMPs

A scanning electron microscope (SEM; S–4300CX; Hitachi, Japan) was used to analyze the morphology of the prepared NMPs. A Fourier-transform infrared spectroscopy (FT-IR) analysis of the NMPs was carried out with a FT-IR spectrophotometer (ISF 66/S, Bruker) to define the various functional groups of the NMPs. An X-ray photoelectron spectroscopy (XPS) examination of the NMPs was done using an Escalab–210 electron spectrophotometer (Spain) to identify the different elements existing on the surfaces of the NMP nanoparticles. A transmission electron microscopy (TEM) analysis of the particles was carried using a TEM model H-8100 by Hitachi. Samples were prepared by dropping a few droplets of a diluted NMP solution onto carbon-coated copper grids.

2.5. Kinetic Study

The rate of MB degradation by NMPs was verified by a pseudo-first-order reaction model [13, 22],

$$ln(C_t/C_0) = -kt \quad (2)$$

where C_0 represents the original concentration of MB (mg/L), C_t is the residual concentration of MB at time t (min), and k is the pseudo-first-order rate constant (min^{-1}).

The removal of the MB by NMPs was also examined by a pseudo-second-order reaction kinetics [23],

$$1/C_t = (1/C_0) + k_2 t \quad (3)$$

The slope of the plot between $1/C_t$ and time yields the pseudo-second-order rate constant k_2.

3. Results and Discussion

3.1. Characterization of NMPs

Fig. 1(a) and Fig. 1(b) show SEM images of the NMPs before and after the reaction. The diameter of the NMPs was found to be less than 100 nm. The SEM analysis revealed that the particles were not spherical in shape before or after the reaction. Moreover, they showed some clumping due to the magnetic interaction with the Fe in the nanoparticles [23]. A SEM-EDX elemental analysis of the NMPs revealed that the contributions of different elements to the total mass, in this case Fe, C, Zn, Al, Si, Cu, Mn, Pb, and Cr, were 63.7, 21.4, 7.8, 2.3, 2.0, 1.3, 0.9, 0.6, and 0.09%, respectively. However, the composition of the elements changed after the reaction, as follows: Fe-47.1%, O-33.0%, Si-6.2%, Cl-4.3%, Zn-3.8% and Al-3.5%. Fig. 1(c) shows a TEM image of the NMPs before the reaction. Particles were formed in a chain-like structure.

Fig. 2 shows the FT-IR spectra of the NMPs before and after the reaction with MB. Metal oxide (M-O) bands were observed on the surfaces of the NMPs before the reaction at 1,389.8 cm^{-1}. However, after the reaction, this peak was found to be smaller and to have shifted to 1,417.1 cm^{-1}. The M-O band represents the presence of MO, M_2O_3 and M_3O_4, indicative of the partial oxidation of the NMPs [24]. The spectra of the NMPs exhibited a widened band at 3,301 cm^{-1}, which can be attributed to O-H stretching [25]. The peak at 2,935.8 which appeared after the reaction may represent the stretching vibration of C–H in the CH_3 and CH_2 groups [26]. The two peaks at 1,638.8 and 1,661.1 cm^{-1} are attributed to O–H bending vibrations [27].

XPS was applied to determine the surface chemical compositions of the NMPs. As shown in Fig. 3, the XPS analyses results revealed that Fe, Zn, N, Ca, C and O existed on the surfaces of the NMPs. The presence of O could be explained by the presence of the oxide forms of the metals on the surfaces, with very little residual ethanol on the surfaces of the NMPs. As shown in Fig. 4(a), XPS spectrum of Fe 2p shows the three peaks. These peaks are corre-

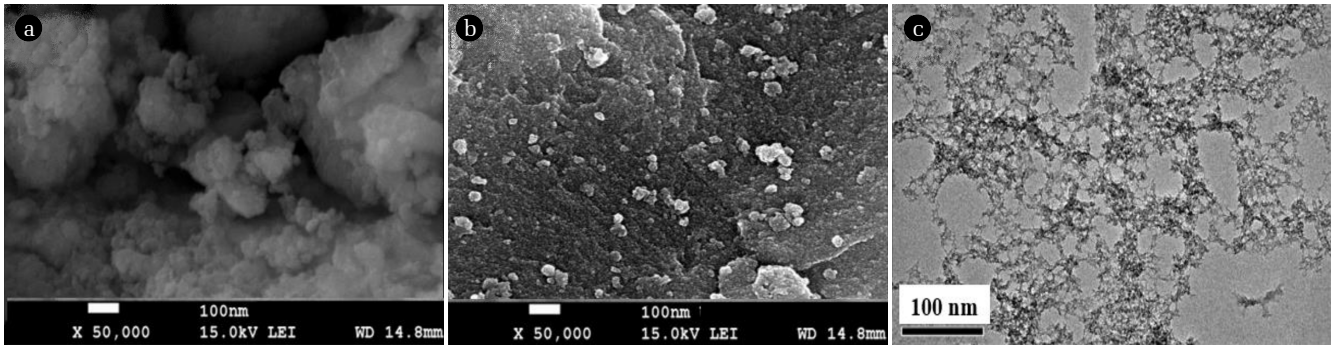

Fig. 1. SEM image of NMPs: (a) before the reaction, (b) after the reaction and (c) TEM image of NMPs.

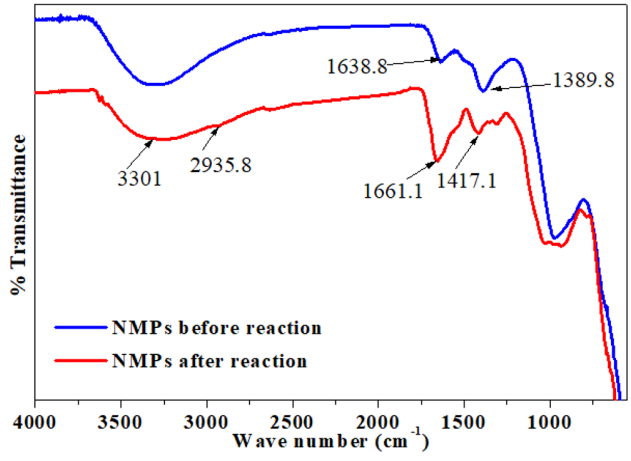

Fig. 2. FTIR spectra of NMPs before and after the reaction with MB.

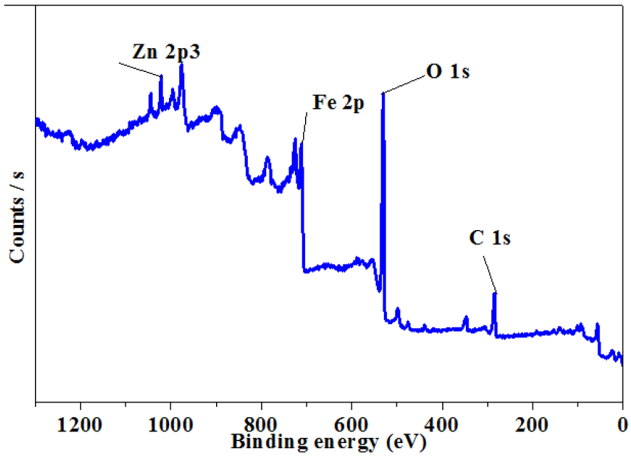

Fig. 3. XPS survey spectra of NMPs.

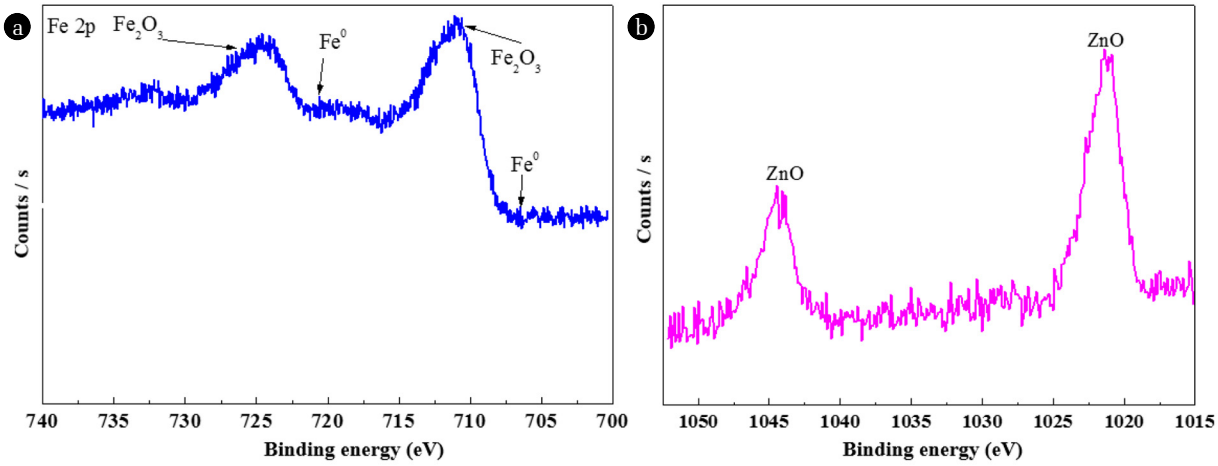

Fig. 4. XPS spectra of Fe 2p (a) and XPS spectra of Zn 2p (b).

sponding to Fe^0, FeO/F_2O_3 (Fe 2p3/2) and Fe_2O_3 (Fe 2p1/2) with binding energies (BEs) of 720.6 eV, 710.6 eV and 724.7 eV, respectively [20]. The XPS spectra of Zn 2p in Fig. 4(b) shows two peaks at the BEs of 1,021.3 and 1,044.5 eV, these peaks could be assigned to ZnO [28]. An XPS spectrum of C1s represents the peaks at 284.9 eV, which assigned to C-C/C-H [29]. However, the XPS spectrum of O1s shows the peak at 530.5 eV, is ascribed to the availability of an oxides in the NMPs [30]. The XPS spectrum of Ca 2p displays the peak at 347.57 eV, which assigned to calcium carbonate or elemental form of Ca. Metals were existed on the surface of NMPs in the form of elements, oxides of metals and carbonates of metals. The XPS analysis could not identify the presence of Si, Mn or Cu on the surfaces of the nanoparticles, likely due to their low concentrations in the samples [13].

3.2. Degradation of MB by NMPs

3.2.1. Effects of the NMP dosage on the MB degradation outcome

There was no MB removal observed with only H_2O_2 (without addition of NMPs), which shows that H_2O_2 alone cannot remove MB and it could not oxidize in this condition. The effects of various NMP dosages (0, 0.075, 0.15, 0.25 and 0.50 g/L) on the reaction rate were studied under the following experimental conditions: a pH of 3.0, an initial MB concentration of 10 mg/L, a temperature of 25°C, and a concentration of H_2O_2 of 100 mM (Fig. 5). With an increase in the NMP dosage, the degradation efficiency of MB improved significantly due to the increased number of reaction sites with an increased concentration of NMPs [13]. Degradation efficiency of MB of nearly 99.6% was achieved at a reaction time of 180 min with a dose of 0.15 g/L (Fig. 6(a)). However, the degradation efficiency decreased slightly (99.1%) at a NMP dose of 0.5 g/L. This result can be explained by the clustering of the NMPs during the reaction [31]. The MB removal was increased with the increase of the NMPs concentration may be due to more availability of reactive site for electron transfer from the surface NMPs to H_2O_2 [12]. NMPs are very capable of degrading MB owing to their small size and greater surface area. On the basis of these results, the optimum dosage of NMPs was determined to be 0.15 g/L

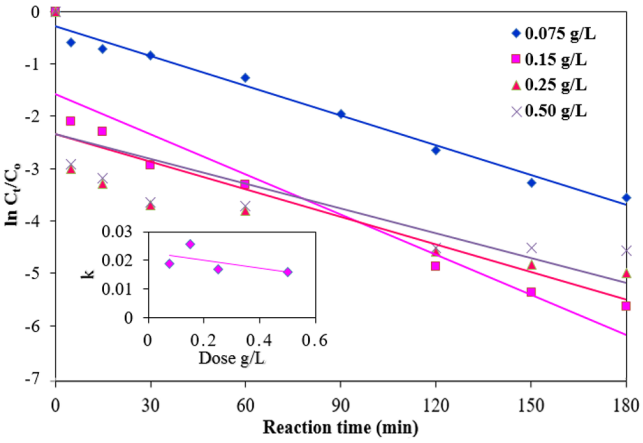

Fig. 5. Effects of the NMP dosage on the degradation of MB. Inset: correlation between the pseudo-first-order rate constant (k) and the NMP dosage.

for the subsequent MB degradation processes. The inset in Fig. 5 shows a plot of the pseudo-first-order rate constant for the removal of MB versus the NMP dosage, indicating that the k_1 value initially increased with the dose to 0.15 g/L and then decreased linearly as the dose continued to increase. Similar trend was also followed by pseudo-second-order rate constant (k_2) (Table 1). The kinetic data with the selected dosages of NMPs are given in Table 1.

3.2.2. Effects of the pH levels on the MB degradation outcome

Many researchers have been reported that most of AOPs are depend on pH and acidic conditions, which are favorable to the reaction [32-33]. The pH is an important parameter which can affect the degradation process of organic pollutants when nZVMs are used under an acidic condition, creating more reactive sites and resulting in greater degradation of these types of pollutants. However, in a highly acidic condition (pH < 2), rapid corrosion of nZVMs reduces the degradation rate [34]. The effects of different pH values (2.0, 3.0, 4.0, 5.0 and 6.8) on the reaction rate were studied under

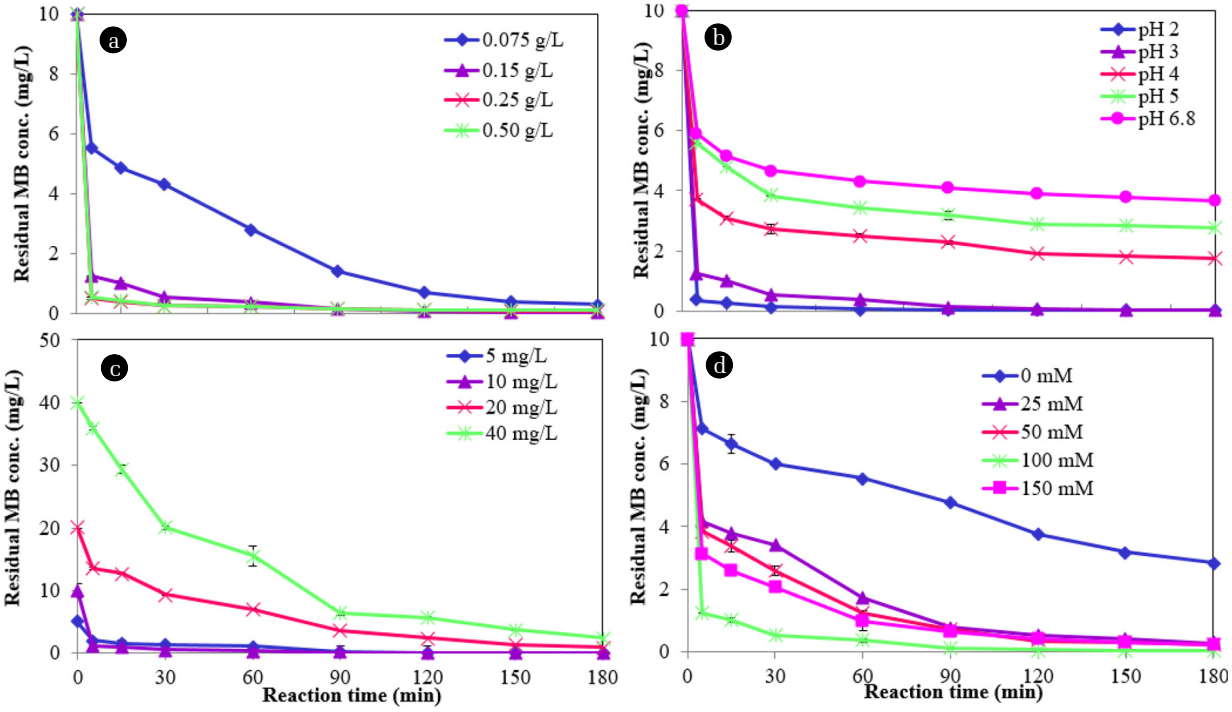

Fig. 6. Effects of different parameters on the MB degradation process: a) effect of the dosage, b) effect of the initial pH value, c) effect of the initial MB concentration and d) effect of the amount of H_2O_2.

Table 1. The Kinetic Results for MB Degradation by NMPs

NMPs dose (g/L)	C_0 (MB) (mg/L)	Initial pH	H_2O_2 conc. (mM)	Pseudo-first-order		Pseudo-second-order	
				k (min^{-1})	R^2	k^2 (L/mg.min)	R^2
0.075	10	3.0	100	0.0189	0.9827	0.0175	0.8797
0.15	10	3.0	100	0.0255	0.8605	0.1473	0.9294
0.25	10	3.0	100	0.0170	0.5880	0.075	0.9829
0.50	10	3.0	100	0.0158	0.5321	0.0516	0.9253
0.15	10	2.0	100	0.0390	0.8141	1.6467	0.6192
0.15	10	4.0	100	0.0052	0.6593	0.0021	0.8336
0.15	10	5.0	100	0.0038	0.6225	0.0012	0.8079
0.15	10	6.8	100	0.0080	0.7307	0.0007	0.7252
0.15	5	3.0	100	0.0347	0.9461	0.3802	0.5601
0.15	20	3.0	100	0.0164	0.9914	0.0051	0.8811
0.15	40	3.0	100	0.0155	0.9805	0.0019	0.918
0.15	10	3.0	0	0.0060	0.9396	0.0013	0.9724
0.15	10	3.0	25	0.0179	0.9470	0.0173	0.949
0.15	10	3.0	50	0.0190	0.9339	0.0225	0.9616
0.15	10	3.0	150	0.0176	0.8950	0.0213	0.9784

the following experimental conditions: an NMP dose of 0.15 g/L, an initial MB concentration of 10 mg/L, a temperature of 25°C, and a H_2O_2 concentration of 100 mM (Fig. 7). The degradation efficiency of MB was found to be greater than 98% within 30 min, then reaching 100% in 180 min at an initial pH of 2.0 (Fig. 6(b)). The degradation efficiency levels of MB were reduced with an increase in the pH from 2 to 6.8 in a reaction time of 180 min. The reduced MB degradation with an increase in the pH to 6.8 can be ascribed the decay of H_2O_2 and the decreased activity of the NMPs [35]. The highest rate of MB degradation was achieved

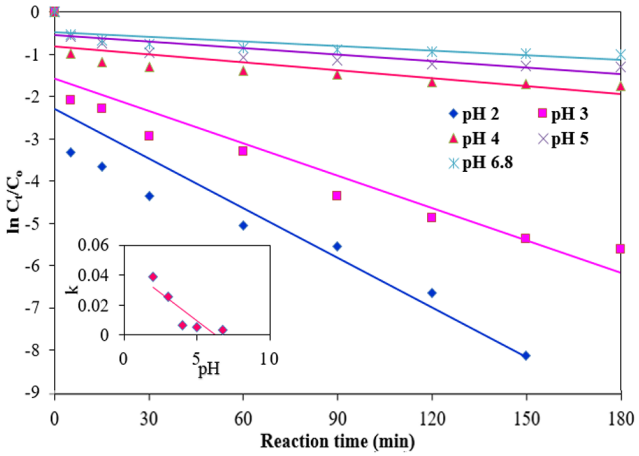

Fig. 7. Effects of different initial pH levels on the degradation of MB. Inset: correlation between the pseudo-first-order rate constant (k) and the pH values.

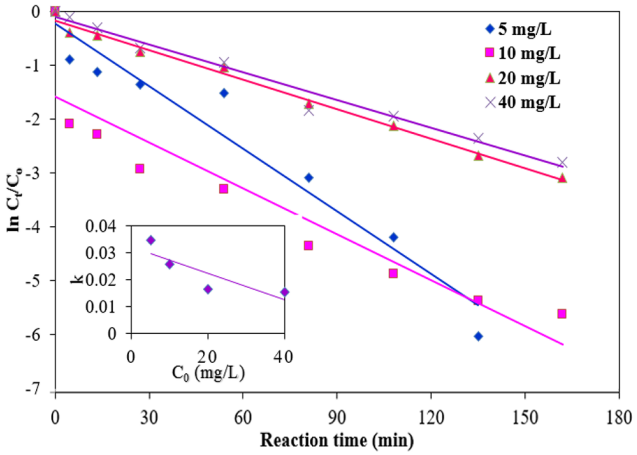

Fig. 8. Effects of different initial MB concentrations on the degradation of MB. Inset: correlation between the pseudo-first-order rate constant (k) and the initial MB concentration.

at pH 2.0, this may be due to releasing metal oxides on the NMP surfaces in an acidic pH; resulting many active sites became available for MB reactions. At pH 4, 5 and 6.8 confined the removal of MB due to the low concentration of H^+ in which is not favourable for the MB removal. Furthermore, metals hydroxides are generated with the increase of the pH from 4 to 6.8 during the process. The accumulation of metal hydroxide precipitates accumulated on the surface of NMPs will hamper the generation of ROS and decrease the MB removal [12].

As shown in Table 1, the value of k_1 was reduced by approximately 90.5%; however, the value of k_2 was reduced 99.96% when the pH was increased from 2 to 6.8. Rapid degradation of MB by the NMPs was observed at a low initial pH of solution. These results also indicate that the reaction rate was significantly decreased with an increase of pH values (inset of Fig. 7). This outcome stems from the fact that the oxides on the surfaces of the NMPs were rapidly dissolved at a low pH and the active sites were free, causing corrosion of the metals, including Fe [12].

3.2.3. Effects of different MB concentrations on the MB degradation outcome

The effects of various initial concentrations of MB (5, 10, 20 and 40 mg/L) on the reaction rate were studied under the following experimental condition: a dose of NMPs of 0.15 g/L, an initial pH of 3, a temperature of 25°C, and a H_2O_2 concentration of 100 mM (Fig. 8). The residual MB concentrations were found to be 0.0, 0.04, 0.91 and 2.4 mg/L for initial concentrations of MB of 5, 10, 20 and 40 mg/L, respectively (Fig. 6(c)). The degradation efficiency of MB was reduced from 100 to 85.7% with an increase in the concentration from 5 to 40 mg/L at a reaction time of 180 min. The active surface sites existing on the NMPs for the reaction were limited by increasing the MB concentration. The values of k_1, k_2 and R^2 for the degradation rate of MB with different MB concentrations are given in Table 1. As shown in the inset of Fig. 6, the correlation between k_1 and the initial concentration of MB indicated that the value of k_1 decreased linearly with an increase in the initial MB concentration. The value of k_2 was also reduced approximately 99%, when concentration of MB increased from 5 to 40 mg/L. The reduction of the MB degradation rate can be attributed to the adsorption of MB onto the surfaces of the NMPs, likely blocking the active sites of NMPs and thus diminishing the constant generation of hydroxyl radicals [35].

3.2.4. Effects of the addition of H_2O_2 on the MB degradation outcome

The effects of various amounts of H_2O_2 (0, 25, 50, 100 and 150 mg/L) on the reaction rate were studied under the following experimental condition: A NMP dose of 0.15 g/L, an initial pH of 3, a temperature of 25°C, and an initial MB concentration of 10 mg/L (Fig. 9). The MB degradation rate was very low with NMPs without an addition of H_2O_2, possibly due to the insufficient number of, or unavailability of hydroxyl radicals in the reaction. As shown in Fig. 6(d), the MB degradation efficiency was increased from 71.6 to 99.6% with an increase in the amount of H_2O_2 from 0 to 100 mM due to the generation of considerable numbers of hydroxyl radicals [31, 36]. However, the efficiency was reduced slightly with 150 mM of hydrogen peroxide. This outcome stems from recombinations caused by hydroxyl radicals, the scavenging effect of H_2O_2, and the inhibition of the oxidation of the NMPs by H_2O_2 (Eqs. (4-6)). At high concentrations of H_2O_2, new radical ($HO_2^{\bullet}$) is formed, which is much less reactive than hydroxyl radicals (Eq. (4)) [35]. As shown in Eq. (5), $HO_2^{\bullet}$ involved in destruction of hydroxyl radicals. However, two hydroxyl radicals are combined to form H_2O_2 (Eq. 6).

$$OH^{\bullet} + H_2O_2 \rightarrow HO_2^{\bullet} + H_2O \quad (4)$$

$$HO_2^{\bullet} + OH^{\bullet} \rightarrow H_2O + O_2 \quad (5)$$

$$OH^{\bullet} + OH^{\bullet} \rightarrow H_2O_2 \quad (6)$$

The values of k_1, k_1 and R^2 for MB degradation rates with different concentrations of H_2O_2 are given in Table 1. As shown in the inset of Fig. 9, the values of k_1 increased linearly to a hydrogen peroxide concentration of 100 mM with a small alteration at the

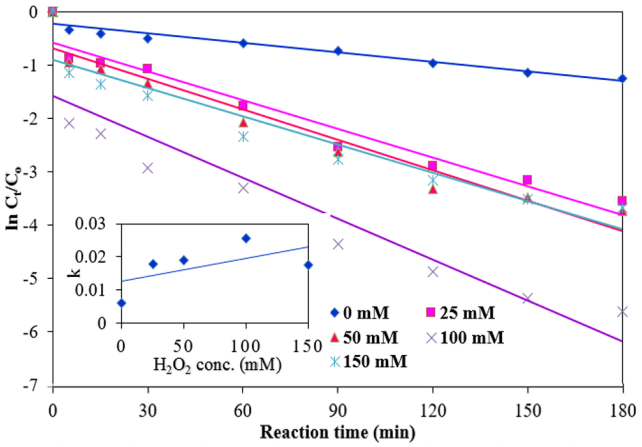

Fig. 9. Effects of different amounts of H_2O_2 on the degradation of MB. Inset: correlation between the pseudo-first-order rate constant (k) and the concentration of H_2O_2.

highest concentration (150 mM). A similar trend was also followed by k_2 values. The degradation of MB was greatly increased with a combination of NMPs and hydrogen peroxide as compared to that solely with NMPs.

3.3. Possible Mechanism for the Degradation of MB by NMPs

The removal characteristics of MB by NMPs with and without H_2O_2 were studied. A low removal rate (71.6%) of MB was achieved by NMPs without the addition H_2O_2. The oxidation of MB by hydroxyl radicals is mainly responsible for the degradation of MB in an aqueous solution. Hydroxyl radicals are produced when an electron migrates from the surface of the NMPs to H_2O_2. The NMPs can react with the available H_2O_2, leading to the generation of further hydroxyl radicals [12-13].

The rapid production of HO^o radicals in an acidic medium occurred during the Fenton-like process, as shown in Eq. (7) [37]. In acidic condition, Fe^0 react with H_2O_2, and then oxidized into Fe^{2+} (Eq. (8)). A Fe^{2+} again react with H_2O_2 and produced Fe^{3+}, $OH^{\bullet}$ and OH^- (Eq. (9)). As expressed by Eq. (10), zero-valent aluminum could react with hydrogen peroxide and produce Al^{3+}, $OH^{\bullet}$ and OH^- [11]. The zero-valent Cu reacts with O_2 in a water system, resulting in Cu^+, H_2O_2, and $OH^{\bullet}$. In an acidic condition, Cu^+ reacts with H_2O_2 and converts into Cu^{2+} along with H_2O, and $2OH^-$ (Eqs. (11-12)) [38]. The degradation of MB takes place by means of oxidizing agents such as H_2O_2 and other oxidative species under an acidic pH and oxic condition, leading to the production of hydroxyl radicals for the decolorization of MB through a Fenton-like process (Eq. (13)) [39-40].

$$NMPs + H_2O_2 + H^+ \rightarrow M^{n+} + OH^{\bullet} + OH^- \quad (7)$$

$$Fe^0 + H_2O_2 + 2H^+ \rightarrow Fe^{2+} + 2H_2O \quad (8)$$

$$Fe^{2+} + H_2O_2 \rightarrow Fe^{3+} + OH^{\bullet} + OH^- \quad (9)$$

$$Al^0 + 3H_2O_2 \rightarrow Al^{3+} + 3OH^{\bullet} + 3OH^- \quad (10)$$

$$2Cu^0 + O_2 + 2H_2O \rightarrow 2Cu^+ + 2OH^- + H_2O_2 \quad (11)$$

$$Cu^+ + H^+ + H_2O_2 \rightarrow Cu^{2+} + 2OH^{\bullet} + H_2O \quad (12)$$

$$OH^{\bullet} + MB \rightarrow Intermediate + CO_2 + H_2O \quad (13)$$

4. Conclusions

NMPs were synthesized from a solution extracted from ASR, these particles were highly effective when used for MB degradation in an aqueous system. The MB degradation rate was improved with an increase in the dosage of the NMPs and the amount H_2O_2 up to a certain limit, past which it decreased gradually. However, the degradation rate decreased with an increase in the pH and the initial MB concentration. The optimum conditions for MB degradation were as follows: a pH of 3.0, an initial MB concentration of 10 mg/L, a NMP dose of 0.15 g/L, 100 mM of H_2O_2, and a temperature of 25°C. The highest removal rate of MB was found to be 100% with an initial MB concentration of 5 mg/L, followed by 99.6% with an initial concentration of 10 mg/L. The pseudo-second-order kinetics was well fitted in comparison to the pseudo-first-order kinetics for the degradation of MB by NMPs. The highest value of k_1 was found to be 0.039 min^{-1} for MB degradation at pH 2. The most probable mechanism for the degradation of MB by NMPs with H_2O_2 was the oxidation of MB by hydroxyl radicals that are generated during the reaction. The present study recommends that MB can be removed successfully through a heterogeneous Fenton-like process.

Acknowledgments

The authors gratefully acknowledge the support of the University Grant Commission (UGC), Government of India (UGC-BSR Research startup grant project No. F. 30-382/2017, BSR). The present research has been conducted by the Research Grant of Kwangwoon University in 2017.

References

1. Zhang X, Cheng L, Wu X, Tang Y, Wu Y. Activated carbon coated palygorskite as adsorbent by activation and its adsorption for methylene blue. *J. Environ. Sci.* (China) 2015:33:97-105.
2. Low FCF, Wu TY, Teh CY, Juan JC, Balasubramanian N. Investigation into photocatalytic decolorisation of CI Reactive Black 5 using titanium dioxide nanopowder. *Color. Technol.* 2012:128:44-50.
3. Li H, Guo J, Yang L, Lan Y. Degradation of methyl orange by sodium persulfate activated with zero-valent zinc. *Sep. Purif. Technol.* 2014;132:168-173.
4. Subramonian W, Wu TY. Effect of enhancers and inhibitors on photocatalytic sunlight treatment of methylene blue. *Water Air Soil Pollut.* 2014;225:1-15.
5. Liu TH, Li YH, Du QJ, et al. Adsorption of methylene blue

from aqueous solution by graphene. *Colloid. Surface. B.* 2012;90:197-203.
6. Han X, Wang W, Ma X. Adsorption characteristics of methylene blue onto low cost biomass material lotus leaf. *Chem. Eng. J.* 2011;171:1-8.
7. Gupta VK, Sharma G, Pathania D, Kothiyal NC. Nanocomposite pectin Zr(IV) selenotungstophosphate for adsorptional/photocatalytic remediation of methylene blue and malachite green dyes from aqueous system. *J. Ind. Eng. Chem.* 2015;25:957-964.
8. Tian BZ, Zhang L, Guo YP, Yan SQ. Enhanced heterogeneous Fenton degradation of methylene blue by nanoscale zero valent iron (nZVI) assembled on magnetic Fe_3O_4/reduced graphene oxide. *J. Water Process Eng.* 2015;5:101-111.
9. Pradhan AA, Gogate PR. Degradation of p-nitro phenol using acoustic cavitation and Fenton chemistry. *J. Hazard. Mater.* 2010;173:517-522.
10. Wang X, Wang L, Li J, Qiu J, Cai C, Zhang H. Degradation of acid orange 7 by persulfate activated with zero valent iron in the presence of ultrasonic irradiation. *Sep. Purif. Technol.* 2014:122:41-46.
11. Weng CH, Huang V. Application of Fe^0 aggregate in ultrasound enhanced advanced Fenton process for decolorization of methylene blue. *J. Ind. Eng. Chem.* 2015;28:153-160.
12. Cheng Z, Fu F, Pang Y, Tang B, Lu J. Removal of phenol by acid-washed zero-valent aluminium in the presence of H_2O_2. *Chem. Eng. J.* 2015;260:284-290.
13. Fang ZQ, Qiu XQ, Chen JH, Qiu XH. Degradation of metronidazole by nanoscale zero-valent metal prepared from steel pickling waste liquor. *Appl. Catal. B. Environ.* 2010;100:221-228.
14. Yang X, Chen W, Huang J, Zhou Y, Zhu Y, Li C. Rapid degradation of methylene blue in a novel heterogeneous Fe_3O_4@ RGO@ TiO_2-catalyzed photo-Fenton system. *Sci. Rep.* 2015;5:1-5.
15. Joseph CG, Li Puma G, Bono A, Krishnaiah D. Sonophotocatalysis in advanced oxidation process: A short review. *Ultrason. Sonochem.* 2009;16:583-589.
16. Singh J, Yang JK, Chang YY. Quantitative analysis and reduction of the eco-toxicity risk of heavy metals for the fine fraction of automobile shredder residue (ASR) using H_2O_2. *Waste Manage.* 2016;48:374-382.
17. Singh J, Lee BK. Pollution control and metal resource recovery for low grade automobile shredder residue: A mechanism, bioavailability and risk assessment. *Waste Manage.* 2015;38: 271-283.
18. Singh J, Lee BK. Reduction of environmental availability and ecological risk of heavy metals in automobile shredder residues. *Ecol. Eng.* 2015;81:76-81.
19. Weng C-H, Huang V. Application of Fe^0 aggregate in ultrasound enhanced advanced Fenton process for decolorization of methylene blue. *J. Ind. Eng. Chem.* 2015;28:153-160.
20. Wang X, Liu P, Fu M, Ma J, Ning P. Novel sequential process for enhanced dye synergistic degradation based on nano zero-valent iron and potassium permanganate. *Chemosphere* 2016;155:39-47.
21. Singh J, Lee BK. Hydrometallurgical recovery of heavy metals from low-grade automobile shredder residue (ASR): An application of an advanced Fenton process (AFP). *J. Environ. Manage.* 2015;161:1-10.
22. Teh CY, Wu TY, Juan JC. Facile sonochemical synthesis of N,Cl-codoped TiO_2: Synthesis effects, mechanism and photocatalytic performance. *Catal. Today* 2015;256:365-374.
23. Singh J, Lee BK. Recovery of precious metals from low-grade automobile shredder residue: A novel approach for the recovery of nano zero-valent copper particles. *Waste Manage.* 2016;48:353-365.
24. Zha SX, Cheng Y, Gao Y, Chen ZL, Megharaj M, Naidu R. Nanoscale zerovalent iron as a catalyst for heterogeneous Fenton oxidation of amoxicillin. *Chem. Eng. J.* 2014;255: 141-148.
25. Singh J, Mishra NS, Uma Banerjee S, Sharma YC. Comparative studies of physical characteristics of raw and modified sawdust for their use as adsorbents for removal of acid dye. *BioResources* 2011;6:2732-2743.
26. Subramonian W, Wu TY, Chai S-P. Using one-step facile and solvent-free mechanochemical process to synthesize photoactive Fe_2O_3-TiO_2 for treating industrial wastewater. *J. Alloys Compd.* 2017;695:496-507.
27. Yuan SJ, Dai XH. Facile synthesis of sewage sludge-derived mesoporous material as an efficient and stable heterogeneous catalyst for photo-Fenton reaction. *Appl. Catal. B. Environ.* 2014;154-155:252-258.
28. Morozov IG, Belousova OV, Ortega D, Mafina MK, Kuznetcov MV. Structural, optical, XPS and magnetic properties of Zn particles capped by ZnO nanoparticles. *J. Alloy. Compd.* 2015;633:237-245.
29. Kim JH, Cho S, Bae TS, Lee YS. Enzyme biosensor based on an N-doped activated carbon fiber electrode prepared by a thermal solid-state reaction. *Sens. Actuators B.* 2014;197:20-27.
30. Dwivedi AD, Dubey SP, Sillanpää M, Kwon YN, Lee C. Distinct adsorption enhancement of bi-component metals (cobalt and nickel) by Fireweed-derived carbon compared to activated carbon: Incorporation of surface group distributions for increased efficiency. *Chem. Eng. J.* 2015;281:713-723.
31. Xu L, Wang J. A heterogeneous Fenton like system with nanoparticulate ZVI for removal of 4 chloro 3 methyl phenol. *J. Hazard. Mater.* 2011;186:256-264.
32. Bokare AD, Choi W. Zero-valent aluminum for oxidative degradation of aqueous organic pollutants. *Environ. Sci. Technol.* 2009;43:7130-7135.
33. Liu WP, Zhang HH, Cao BP, Lin K, Gan J. Oxidative removal of bisphenol A using zero valent aluminum-acid system. *Water Res.* 2011;45:1872-1878.
34. Tian H, Li JJ, Mu Z, Li LD, Hao ZP. Effect of pH on DDT degradation in aqueous solution using bimetallic Ni/Fe nanoparticles. *Sep. Purif. Technol.* 2009;66:84-89.
35. Babuponnusami A, Muthukumar K. Removal of phenol by heterogeneous photo electro Fenton-like process using nano-zero valent iron. *Sep. Purif. Technol.* 2012;98:130-135.
36. Subramonian W, Wu TY, Chai S-P. Photocatalytic degradation of industrial pulp and paper mill effluent using synthesized magnetic Fe_2O_3-TiO_2: Treatment efficiency and characterizations of reused photocatalyst. *J. Environ. Manage.* 2017;187:298-310.
37. Asghar A, Abdul Raman A, Daud WM. Advanced oxidation processes for insitu production of hydrogen peroxide/hydroxyl

radical for textile wastewater treatment: A review. *J. Clean. Prod.* 2015;87:826-838.
38. Dong G, Ai Z, Zhang L. Total aerobic destruction of azo contaminants with nanoscale zero-valent copper at neutral pH: Promotion effect of in-situ generated carbon center radicals. *Water Res.* 2014;66:22-30.
39. Yang S, Wang P, Yang X, Shan L, Zhang W, Shao X, Niu R. Degradation efficiencies of azo dye Acid Orange 7 by the interaction of heat, UV and anions with common oxidants: Persulfate, peroxymonosulfate and hydrogen peroxide. *J. Hazard. Mater.* 2010;179:552-558.
40. Singh J, Yang JK, Chang YY. Rapid degradation of phenol by ultrasound-dispersed nano-metallic particles (NMPs) in the presence of hydrogen peroxide: A possible mechanism for phenol degradation in water. *J. Environ. Manage.* 2016;175:60-66.